Journal Pre-proof



Quantitative phosphoproteomics analysis uncovers PAK2 and CDK1 mediated malignant signaling pathways in clear cell Renal Cell Carcinoma

Aydanur Senturk, Ayse T. Sahin, Ayse Armutlu, Murat Can Kiremit, Omer Acar, Selcuk Erdem, Sidar Bagbudar, Tarik Esen, Nurhan Ozlu

PII: S1535-9476(22)00225-0

DOI: https://doi.org/10.1016/j.mcpro.2022.100417

Reference: MCPRO 100417

To appear in: *Molecular & Cellular Proteomics*

Received Date: 12 September 2021

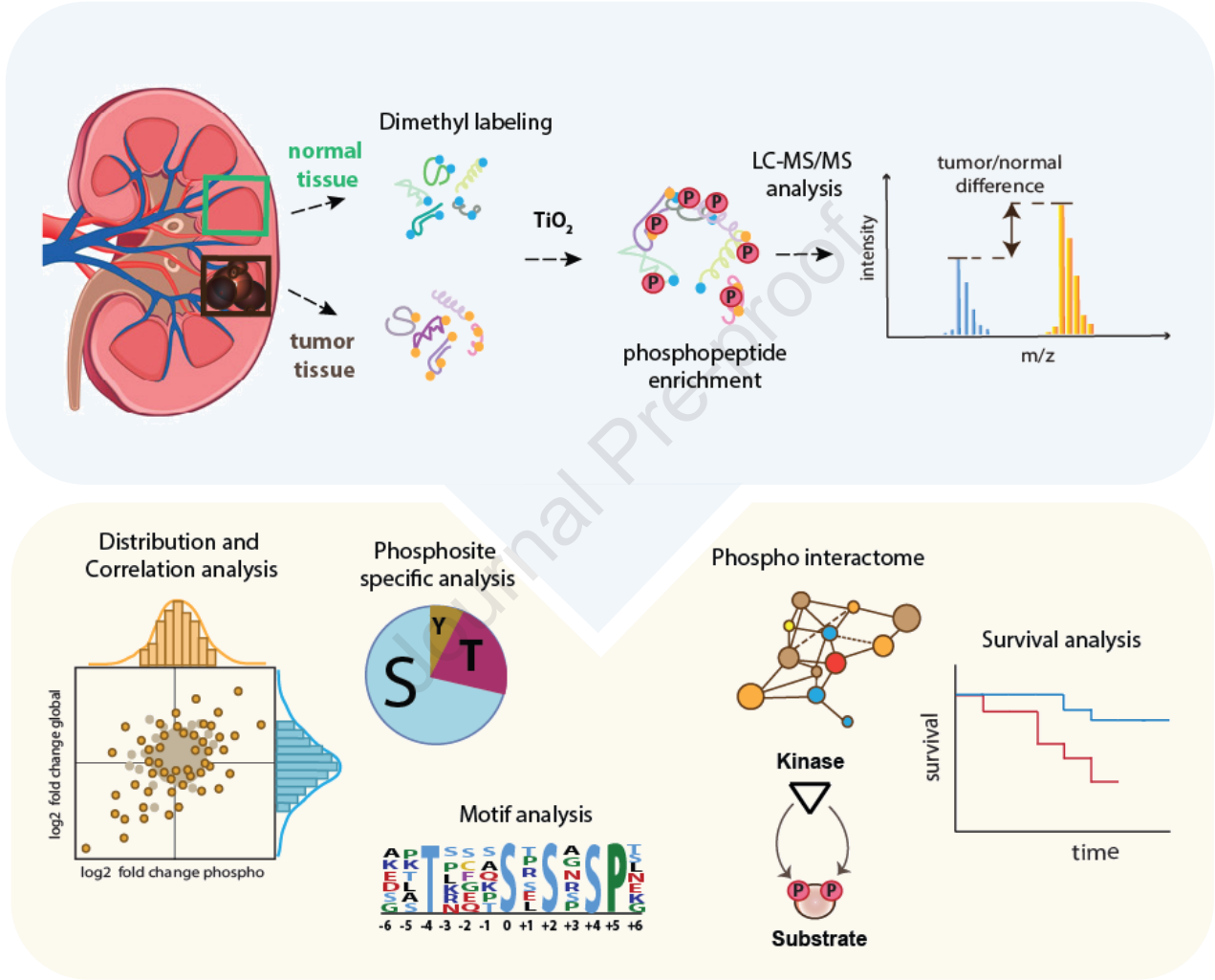
Revised Date: 23 August 2022

Accepted Date: 19 September 2022

Please cite this article as: Senturk A, Sahin AT, Armutlu A, Kiremit MC, Acar O, Erdem S, Bagbudar S, Esen T, Ozlu N, Quantitative phosphoproteomics analysis uncovers PAK2 and CDK1 mediated malignant signaling pathways in clear cell Renal Cell Carcinoma, *Molecular & Cellular Proteomics* (2022), doi: https://doi.org/10.1016/j.mcpro.2022.100417.

This is a PDF file of an article that has undergone enhancements after acceptance, such as the addition of a cover page and metadata, and formatting for readability, but it is not yet the definitive version of record. This version will undergo additional copyediting, typesetting and review before it is published in its final form, but we are providing this version to give early visibility of the article. Please note that, during the production process, errors may be discovered which could affect the content, and all legal disclaimers that apply to the journal pertain.

© 2022 THE AUTHORS. Published by Elsevier Inc on behalf of American Society for Biochemistry and Molecular Biology.



Journal Pre-proof

Journal Pre-proof

Quantitative phosphoproteomics analysis uncovers PAK2 and CDK1 mediated malignant signaling pathways in clear cell Renal Cell Carcinoma

Aydanur Senturk[1], Ayse T. Sahin[1], Ayse Armutlu[2], Murat Can Kiremit[3], Omer Acar[3], Selcuk Erdem[4], Sidar Bagbudar[5], Tarik Esen[3] and Nurhan Ozlu[1,6]*

[1] Department of Molecular Biology and Genetics, Koc University, 34450, Istanbul, Turkey

[2] Department of Pathology, Koc University School of Medicine, 34010, Istanbul, Turkey

[3] Department of Urology, Koc University School of Medicine, 34010, Istanbul, Turkey

[4] Department of Urology, Istanbul University, Istanbul Faculty of Medicine, 34093, Istanbul, Turkey

[5] Department of Pathology, Istanbul University, Istanbul Faculty of Medicine, 34093, Istanbul, Turkey

[6] Koc University Research Center for Translational Medicine (KUTTAM), 34450, Istanbul, Turkey

*Correspondence should be addressed to Nurhan Ozlu (email: nozlu@ku.edu.tr), Koc University, Department of Molecular Biology and Genetics, 34450, Turkey, +90 212 338 1571

Running title: Phosphoproteome analysis of ccRCC

Conflict of interest statement: The authors declare no potential conflicts of interest.

Journal Pre-proof

Journal Pre-proof

Abstract

Clear cell Renal Cell Carcinoma (ccRCC) is among the 10 most common cancers in both men and women and causes more than 140,000 deaths worldwide every year. In order to elucidate the underlying molecular mechanisms orchestrated by phosphorylation modifications, we performed a comprehensive quantitative phosphoproteomics characterization of ccRCC tumor and normal adjacent tissues. Here, we identified 16,253 phosphopeptides, of which more than 9,000 were quantified. Our in-depth analysis revealed 600 phosphopeptides to be significantly differentially regulated between tumor and normal tissues. Moreover, our data revealed that significantly up-regulated phosphoproteins are associated with protein synthesis and cytoskeletal re-organization which suggests proliferative and migratory behavior of renal tumors. This is supported by a mesenchymal profile of ccRCC phosphorylation events. Our rigorous characterization of the renal phosphoproteome also suggests that both EGFR and VEGFR are important mediators of phospho signaling in RCC pathogenesis. Furthermore, we determined the kinases PAK2, CDK1 and JNK1 to be master kinases that are responsible for phosphorylation of many substrates associated with cell proliferation, inflammation and migration. Moreover, high expression of PAK2 is associated with worse survival outcome of ccRCC patients. These master kinases are targetable by inhibitory FDA-approved drugs such as fostamatinib, minocycline, tamoxifen and bosutinib which can serve as novel therapeutic agents for ccRCC treatment.

Keywords: phosphoproteomics, Renal Cell Carcinoma, PAK2, drug targets, signaling pathways

Journal Pre-proof

Journal Pre-proof

Introduction

Clear cell Renal Cell Carcinoma (ccRCC) is the most common (~75% frequency) and most malignant histological subtype of kidney cancer caused primarily by loss of the tumor suppressor von-Hippel-Lindau (*VHL*) gene (1). The disease accounts for more than 140,000 deaths worldwide every year (2) and is characterized by a 5-year survival rate of <10% for advanced tumors (3). Despite the increasing interest in understanding the pathogenesis of this cancer type, RCC is still mainly treated by surgical resection of the tumor mass as it is considered to be resistant to traditional chemotherapy and radiotherapy (2). In recent years, high-throughput mass spectrometry-based phosphoproteomics analysis of cancer biopsies has emerged as promising tool to elucidate the underlying molecular mechanisms of tumor pathology. Phosphorylation is the most common and most important reversible post-translational modification (4). It is assumed that around 75% of the human proteome is transiently phosphorylated in order to regulate and maintain biological processes such as cell division, protein synthesis, cell growth, apoptosis and development (4, 5). In fact, kinases, which are in many cases enzymes or receptors, are attractive targets for numerous FDA-approved drugs (4, 6). However, attempts to portray the phosphorylation profile of ccRCC tumors are scarce. Deb and colleagues (7) conclude by comparing the respective Clinical Proteome Tumor Analysis Consortium (CPTAC) data that the ccRCC phosphoproteome is in general distinct from that of 5 other cancer types, as lower abundance levels for 161 common phosphosites were determined in RCC. Furthermore, the CPTAC phosphoproteome of ccRCC (8) includes more than 40,000 identified phosphosites detected by Fe^{3+}-IMAC (immobilized metal affinity chromatography) and represents, besides the study of Peng and colleagues (9), one of the largest phospho-profiles of ccRCC tissues. However, while the CPTAC analysis uncovered druggable phosphorylation signaling events such as the EGFR-mediated MAPK and AKT1-mTOR pathways, Peng and colleagues were rather interested in the general identification of missing proteins (evidenced only at the transcript level, but predicted at the protein level). Another attempt described by Haake and colleagues (10) aimed to characterize

Journal Pre-proof

tyrosine phosphorylations by pY-immunoprecipitation in ccRCC tissues and cell lines, respectively. Elevated tyrosine phosphorylation profiles were determined for the EGFR, MAPK as well as the FAK pathways in the different biospecimens, which can be effectively targeted by various tyrosine-kinase inhibitors (10).

Here, we performed dimethylation-based quantitative phosphoproteomics analysis of ccRCC tissues to illuminate previously undescribed signaling cascades. For the phosphopeptide enrichment, we employed on-column TiO_2-MOAC (metal oxide affinity chromatography) and detected more than 16,000 phosphopeptides. Our approach revealed that besides the MAPK and EGFR pathways, a VEGFR-induced pathway is strongly activated in the tumor tissues leading to the activation of multiple CDK and PAK kinases. Our findings suggest that these events drive tumor growth, progression and invasion.

Experimental Procedures

Ethics statement

The study proposal was approved by the Ethics Committee of Koc University in September 2017 (no. 2017.145.IRGB2.051) and was prolonged for two more years. Tissue samples were collected with the patients' informed written consent following the guidelines of the Declaration of Helsinki.

Sample collection

The same tumor and matched normal adjacent tissue (NAT) samples of the discovery cohort from our previous publication were used for phosphoproteomics analysis (11). The age of the 13 patients varied between 47 and 74 and reflected a typical gender representation for RCC with a 1.6:1 male-to-female-ratio (**Supplementary File S1**). Resected tissue samples were reached to the pathologist within 10 min and viable tumor areas were immediately sectioned

Journal Pre-proof

and stored at -80°C for subsequent pathological evaluation and proteomics sample preparation (**Fig. S1**).

Experimental Design and Statistical Rationale

For quantitative phosphoproteomics analysis, proteins from 13 frozen tumor and normal tissue biospecimens, respectively, were isolated and subjected to LC-MS/MS analysis. The order of sample preparation was randomized and independent of the patient list (**Supplementary File S1**). The same processed peptide samples that were used for global proteome analysis in our previous publication (11) were used in this study for phosphoproteomics characterization. To prevent bias from the chemical labeling of peptide samples (dimethylation), the labeling was swapped for half of the patient samples. Phospho-enriched samples were analyzed as triplicates and the total set of identified phosphopeptides was subjected to multiple filtration steps to reduce the data into “high-confidence” (quantified in ≥75% of the cohort, Tier I) and “medium-confidence” (quantified in ≥50% of the cohort, Tier II) phosphopeptides. For comparative analysis the obtained phosphopeptides were compared to different databases such as PhosphoSitePlus, CPTAC (ccRCC) and TCGA-KIRC, respectively. To determine significantly regulated phosphopeptides between tumor and normal tissues, one-sample Wilcoxon signed-rank test (p-value <0.05) was employed on the median $\log_2$ tumor/normal ratios.

In-solution digest, isotopic labeling and fractionation of samples

Sample preparation steps including protein digest, peptide labeling and fractionation are described in our previous study (11). Briefly, NAT and tumor tissue samples were subjected to protein isolation using a urea based lysis buffer followed by extensive homogenization in a bullet blender. Trypsinized samples were then labeled at their primary amines (N-terminus and lysine residues) with heavy and light dimethyl isotopes to incorporate a fixed mass difference between sample types. Labeling reagents were swapped for half of the samples in order to prevent bias from the labeling choice (**Supplementary File S1**). After mixing the labeled

Journal Pre-proof

samples of a patient at 1:1 heavy-light-ratio, the peptide mixtures (estimated protein amount 1.2 mg) were fractionated on-column by Strong Cation Exchange (SCX) chromatography into 10 fractions. Desalted fractions were stored at -20°C.

Phosphopeptide enrichment

Enrichment of phosphopeptides was performed on-column by MOAC using 500 µg of titanium dioxide (TiO_2) beads (5 µm, Sachtleben) packed into micro-columns (20 µL GELoader, eppendorf), which were equilibrated with loading buffer (80% acetonitrile (ACN) and 6% trifluoroacetic acid (TFA)) (12). The dried desalted dimethyl-labeled peptide fractions were reconstituted in loading buffer to a final concentration of 1 µg/µL and the 10 fractions were pooled into 6 fractions. The peptides were slowly loaded onto the positively charged micro-columns at 50*g*. The bound phosphopeptides were washed with 0.1% TFA in 50% ACN and then eluted with 20 µL of 10% ammonia solution into a new tube containing 35 µL of 10% formic acid (FA). The eluted peptides were further acidified by addition of 3 µL of 100% FA and immediately analyzed in LC-MS/MS.

Data acquisition

The phospho enriched fractions were analyzed in triplicate with a 120 min linear gradient on an UltiMate 3000 RSLCnano reversed phase chromatography platform (Thermo Fisher Scientific) coupled to a Q Exactive HF hybrid quadrupole-Orbitrap mass spectrometer (Thermo Fisher Scientific). The fractions were loaded onto an in-house packed 100 µm i.d. × 17 cm C18 column (Reprosil-Gold C18, 5 µm, 200Å, Dr. Maisch) and run with a flow rate of 300 nL/min. The chromatographic separation of the peptides started at 4% of solution B (ACN with 0.1% FA) and gradually increased to 25% in 67 min. The gradient continued from 25% to 45% of solution B in the next 20 min. Peptides in the mass range of 400−1,500 m/z and with a positive polarity were allowed for detection in data-dependent mode. For the MS1 spectra acquisition the resolution was set to 120,000, the automatic gain control (AGC) target to 1e6 and the maximum injection time to 60 ms. The top 20 most intense peptides per cycle were selected for fragmentation in the higher-energy collisional dissociation (HCD) cell with a normalized

Journal Pre-proof

collision energy (NCE) of 27. MS2 spectra acquisition was conducted at a resolution of 30,000, an AGC target of 1e5, a maximum injection time of 60 ms and a fixed first mass of 100 m/z. Furthermore, the isolation window was set to 2.0 m/z, the dynamic exclusion to 20 s, the minimum AGC to 3e3 and the charge exclusion was set as unassigned, 1.

Data processing

Peptide identification and quantification from raw MS data files were done with Proteome Discoverer (PD) (v1.4, Thermo Scientific) using the Mascot (v2.5.1, Matrix Science) search engine. The peptide spectral matches were searched against a Swissprot database containing 21,039 entries for *Homo sapiens* retrieved from Uniprot in March 2016. Trypsin was selected as hydrolytic enzyme with a maximum number of allowed missed cleavages of 2. For peptide identification a mass tolerance of ±20 ppm for precursor masses and ±0.05 Da for fragment ions was selected. For dimethyl labeling the 2plex dimethyl-based heavy/light quantitation method with a mass precision requirement of 2 ppm for precursor ions was used. Light and heavy dimethylation of peptide N termini and of lysine residues, phosphorylation at serine, threonine and tyrosine residues, as well as methionine oxidation were set as dynamic modifications. Cysteine carbamidomethylation was set as fixed modification. Determination of phosphosite positions was done by using the implemented node phosphoRS (v3.0). The False Discovery Rates (FDR) for peptide and protein identifications were set to 1% using the Percolator node in PD (13). Furthermore, a filter was applied to allow only peptide identifications with medium and high confidence, with a sequence length between 7 and 25, a Mascot score >20 and a peptide rank of 1.

Quantification ratios of samples with swapped dimethyl labeling were converted to tumor/normal format. The data was filtered for peptides quantified in at least 2 out of 3 technical replicates in any of the 13 biological replicates. The 3,810 resulting phosphopeptides are hereafter denoted as “quantified phosphopeptides”. A second filter was applied to reduce the data to phosphopeptides quantified in ≥75% of the cohort (Tier I) or ≥50% of the cohort (Tier

Journal Pre-proof

II). All quantification ratios were then normalized to the median of the non-phosphorylated peptides in the sample and $\log_2$ transformed. The phosphorylated peptides were further filtered for ≥50% phosphosite probability.

For statistical analysis the Python function scipy.stats.wilcoxon (v0.14.0) was extended by the feature to omit missing quantification values, and was then applied peptide-wise on the whole technical replicates data. *P*-values <0.05 were considered statistically significant which led to a total of 600 (Tier I) and 1,223 (Tier II) "significantly regulated phosphopeptides", respectively. All subsequent analyses were performed with the Tier I dataset unless otherwise stated.

For the determination of statistical difference between phospho- and non-phosphopeptide distributions, two-sample Student's *t*-test (*p*-value <0.05) was applied via the Python function scipy.stats.ttest_ind.

Functional annotation

Significantly up- and down-regulated phosphorylated proteins were annotated by their Gene Ontology (GO) biological process association using the PANTHER (v14) platform (14) with an FDR setting of 0.05. The proteins were further annotated by their function in cancer using the COSMIC Cancer Gene Census database (v91) (15), and also by associated FDA-approved drugs with inhibitor function retrieved from the Drugbank database (v5.1.7, access August 2020) (16), respectively. Chemical elements were excluded as drugs.

To further characterize the functionality of the phosphopeptides, a previously published study from our group on the epithelial-to-mesenchymal phosphoproteome (17) was used for sequence-based comparison with the determined significantly dysregulated phosphopeptides.

Moreover, we assessed for the significant phosphopeptides the probability of biological relevance by using the data of Ochoa and colleagues (18) and annotating the phosphopeptides by their reported functional score. More specifically, both datasets were matched by the protein sequence position and the residue type of the modification, respectively. Only phosphopeptides with a score >0.5 were considered functional.

Kinase-substrate network recreation

To predict kinase activities in the tumor and NATs, we implemented the NetworKIN3.0 (19) algorithm (access August 2022), which annotates kinases based on STRING interactions and phylogenetic links within kinase families. For this purpose, the significantly regulated phosphopeptides of the Tier II dataset were centered to their phosphosite and expanded by the surrounding ±7 amino acid (aa) sequence window. Only kinase-substrate predictions with a NetworKIN score >5 were considered for network recreation using the visualization software Cytoscape (v3.8.0). The network components were annotated by their GO cellular compartment feature using QuickGO (20), limited only to Uniprot assignments. In case of multiple cellular allocations, priority was given as follows: “membrane”, “nucleus”, “cytoplasm”, “extracellular” and “other”, respectively. Additionally, the recreated network was complemented with the enriched Reactome pathways retrieved as over-representation analysis (ORA) of the kinases and substrates via the webtool WebGestalt (v2019) (21) (access August 2022) at default settings.

The predicted kinases were further mapped to the human kinome phylogenetic tree using the $KinMap_{beta}$ tool at www.kinhub.org (access August 2022) (22).

Motif and survival analysis

To find conserved sequence motifs, the ±7 aa sequence windows of the centered significantly regulated phosphosites were subjected to the webtool MoMo (v5.3.3) (23) (access August 2022), which applies the motif-x algorithm. For the predictions a 15 residue motif width, 20 occurrences and a *p*-value of <0.000001 were set.

For the determination of the prognostic power of kinases, the web tool Kaplan-Meier Plotter (24) (access August 2022) was used with the mRNA data of The Cancer Genome Atlas Kidney Renal Clear Cell Carcinoma (TCGA-KIRC) cohort (n=530) (25), and the “auto select best cutoff” option to optimally partition the patients based on the lowest *p*-value and the highest hazard ratio.

Journal Pre-proof

Additionally, the proteome data of the CPTAC cohort (n=102) (8) was used for survival analysis. For this purpose, the CPTAC global proteome and phosphoproteome data were processed by removing control samples, non-ccRCC samples and contaminated samples, respectively. Furthermore, the phosphopeptide data was aggregated to obtain phosphoprotein quantification values by calculating the mean abundance value from all quantified phosphopeptides of a protein in a sample. Individual tumor quantification values were then gene-wise normalized to the median quantification value of all normal tissue samples. Partitioning of the CPTAC cohort into “low and high expression” was based on the mean quantification value of the kinase of interest as cut-off. Survival curves were created using the KaplanMeierFitter and multivariate_logrank_test functions of the Python library lifelines (v0.25.0).

Comparison with other data

The generated phosphoproteomics data was compared with the corresponding global proteome data of the same tissue samples previously described by our group (11). More specifically, the median $\log_2$ tumor/normal ratio for a given phosphopeptide was compared with the respective ratio of the available non-phosphorylated version of the peptide.

The identified phosphosites of this study were also compared with the PhosphoSitePlus database (access November 2020) (26) by matching the ±7 aa sequence windows. We further compared our ccRCC phosphoproteome with the processed CPTAC data (8) by matching protein sequence positions of identified individual phosphosites. Furthermore, the phosphosite datasets were also compared quantitatively by their median $\log_2$ tumor/normal ratios (CPTAC cohort with both tumor and matched normal tissue samples, n=80). Pearson and Spearman correlations were calculated for common quantified phosphosites using the respective Python scipy.stats functions.

Cell viability assay

Journal Pre-proof

Approximately 7,500 cells (CAKI-2, A498 and MCF7) were seeded in 96-well cell culture plates and treated with different concentrations of tamoxifen for up to 72 h. After each 24-hour treatment with the drug, the cells were fixed with 50% trichloroacetic acid for 1 h at +4°C. Viable cells were stained for 30 min at room temperature using 0.4% Sulforhadamine B solution and washed with 1% acetic acid. 10 mM Tris solution was then added to the wells and the optical density was measured at 564 nm in a Thermo Scientific MultiskanGO plate reader. For each individual experiment, cell survival changes were expressed as percent of the untreated control. Statistical analysis was done using two-way ANOVA in GraphPad PRISM v9.

Results

Shotgun proteomic approach achieves deep coverage of ccRCC phosphoproteome

In this study, a comprehensive quantitative phosphoproteomics analysis of frozen ccRCC tumors and normal adjacent tissues has been conducted to illuminate undiscovered signaling pathways mediated by protein phosphorylation. For this purpose, the dimethyl-labeled fractionated peptides of tumor and NATs from our previous global proteomics analysis (11) were subjected to phosphopeptide enrichment using TiO_2 beads and were analyzed as technical triplicates in LC-MS/MS (**Fig. 1A**). The discovery cohort consisted of 13 patients of different age, grade, stage and gender. In general, the identification and quantification of phosphorylated and non-phosphorylated peptides in the enriched samples were robust across patients and spanned approximately 12 orders of magnitude in the tumor/normal fold change dynamic range (**Fig. 1B**). In total, we identified 16,253 phosphopeptides from the tumor and NAT samples with an FDR of 0.01, which were assigned to 3,486 phosphoproteins (**Fig. 1C**). The majority of the identified phosphosites (15,136) were class I sites with a localization probability of ≥75%. Out of these phosphosites 10,811 were unique sites (localization probability cut-off ≥50%). Furthermore, 3,810 dimethyl-labeled phosphopeptides were quantified in both tumor and NATs, which corresponded to 1,329 quantified phosphoproteins.

Journal Pre-proof

In general, the abundance levels of quantified peptides (log_{10} peak area) varied over 4 orders of magnitude in dynamic range (**Fig. 1D**). Moreover, the fold change distributions of quantified phosphopeptides and non-phosphopeptides followed a near normal pattern (**Fig. 1D**, top histogram), however, a significant skewness of phosphopeptide ratios towards positive values was noticeable suggesting enhanced phosphorylation events in the tumor tissues compared to NATs (**Fig. 1E**). As expected, most phosphosites were serine residues (88.4%), followed by threonine (10.6%) and tyrosine residues (1.01%) coinciding with previously reported frequencies (4) (**Fig. 1F**). Furthermore, most peptides were singly phosphorylated (70.3%) while only a small portion of peptides harbored multiple phosphosites, which is also in line with previous observations (9) (**Fig. 1G**). Comparing the identified phosphopeptides of this study with the PhosphoSitePlus database revealed that approximately 80.5% were already reported, implicating that the majority of phosphorylation modifications in kidney cancer are not tissue-specific (**Fig. 1H**).

Significantly regulated phosphorylations play a role in tumor invasion and harbor conserved kinase recognition sites

Out of more than 3,810 quantified phosphopeptides, we determined 600 as statistically differentially abundant between tumors and NATs (Wilcoxon signed-rank test, *p*-value <0.05) (**Fig. 2A**), which were assigned to 323 unique proteins (**Supplementary File S2**). The majority were up-regulated phosphopeptides (**Fig. 2A** and **B**), supporting our observation of elevated phosphorylation events in ccRCC tumors (**Fig. 1E**). Interestingly, the 269 significantly up-regulated phosphoproteins in the tumors were primarily associated with protein synthesis and cytoskeleton organization, while the 60 significantly down-regulated phosphoproteins were associated with actin-filament organization (**Fig. 2C**). These aberrant biological processes suggest an increase in cell growth, cell motility and invasiveness, which are indicators of malignant tumors and have previously been linked to worse patient outcome (27). Among the phosphorylated intermediate filament components were vimentin (**Supplementary File S2**

(Tier I & Tier II)) and several keratins (KRT) such as KRT8 (**Fig. S2A** and **B, Supplementary File S2** (Tier II)) and KRT19 (**Supplementary File S2** (Tier II))**.**

To further understand the effect of phosphorylation, we compared the generated phosphoproteome profile with our global proteome data of the same ccRCC tissues (**Fig. 2D-F**) (11). The majority of the 323 dysregulated phosphoproteins (76.5%) were not significantly regulated at the global proteome level, while 76 phosphoproteins (23.5%) were also significantly regulated on the global level (**Fig. 2D and 2E**). This implies that most of the phosphorylated proteins are similarly abundant between tumor and normal tissues and that the generally low stoichiometry of the phospho-proteoforms is sufficient for molecular impact in the tumor cells such as change in the activity, structure, conformation or localization of proteins (28). To assess whether the phosphorylation modification itself or the general abundance of the peptide was elevated in the tumors, we compared for the 600 significantly regulated phosphopeptides the abundance levels between the phospho- and available non-phosphorylated version (**Fig. 2F**). In total, 204 of the 600 significantly regulated phosphopeptides had a non-phosphorylated counterpart in the global proteome. Indeed, the $\log_2$ tumor/normal ratios of phosphorylated peptides were significantly higher compared to those of the respective non-phosphopeptides (Wilcoxon signed-rank test, *p*-value <0.00001) (**Fig. 2F**), confirming that the observed signaling events are due to phosphorylation of the proteins.

Furthermore, 296 of the 513 significantly up-regulated phosphopeptides were associated with conserved serine recognition sequences (**Fig. 2G** and **H**, **Supplementary File S4**) such as the proline-containing serine motifs xxxxxxxSPxxxSxx and xxxxxxxSPxxxxxx, which are known target sites of the mitotic kinases CDK1 and CDK5, respectively (29). Other frequent kinase target motifs were xxLxRxxSxxxxxxx and xxxxRxxSxxxxxxx, which are associated with different kinase groups such as CaMK, AMPK, PKA and PKCα, respectively (29).

Journal Pre-proof

Journal Pre-proof

CDK1 and PAK2 kinases are highly activated in ccRCC tumors

In order to unveil the most prominent kinase activities, we applied the kinase prediction tool NetworKIN on the determined significantly regulated phosphosites (600 in total, see **Fig. 2A** and **B**). We reduced the predictions to high-confident ones with a NetworKIN score of ≥5 (178 predictions in total). In summary, out of the 323 significantly regulated phosphoproteins, 82 were substrates of a total of 53 different kinases (**Supplementary File S4**). Among the most frequently activated kinases were different CDK kinases such as CDK1 and CDK5 (**Fig. 3A**), which confirms our previous finding that the conserved phosphosite recognition sequences of these kinases are highly enriched (**Fig. 2G** and **H**). Furthermore, PAK2 is the second most activated kinase in the tumor tissues, followed by GSK3 beta and JNK1 (**Fig. 3A**). Also, predictions for the kinases p38b (MAPK11) and p38d (MAPK12) are highly enriched and suggest the activation of the MAPK pathway (8). In contrast, the activity for the kinases TGFbR2, AKT1, PAK1, CaMK2g as well as PDHK2 and PDHK3 was reduced in the tumor tissues compared to NATs. Furthermore, all predicted kinases belonged to serine/threonine families (**Fig. 3B**). The majority of the kinases belonged to the CMGC, AGC and STE families with an overall increased activity in the ccRCC tumors (**Fig. S2C**). Moreover, the rare kinase family PDHK was only associated with reduced phosphorylation events in the tumors.

To illuminate the most prominent signaling pathways in the ccRCC tumors, we recreated the predicted kinase-substrate interactions as network and complemented it with the associated Reactome pathways (Tier II data, **Fig. 3C, Supplementary File S4**), which unveiled that certain malignant processes such as AKT signaling, VEGF signaling, MAPK-related signaling and signaling by interleukins and second messengers shape the pathobiology of renal cancers. Moreover, the activation of RAC1 is the most enriched pathway in the tumors, with all known 6 PAK kinase isoforms predicted to be activated in the tumors (PAK1 and PAK4 are also associated with down-regulated phosphopeptides, **Supplementary File S4**). We further annotated the genes in the network by their role in cancer (colored font) and noticed that several known oncogenes are substrates of the kinases such as EGFR, MAPK1, AKT1, AKT2,

Journal Pre-proof

MAP2K1, MAP2K2, SGK1, BRAF and CDK4. Furthermore, 9 substrates were identified to have a mesenchymal phosphorylation (yellow border) (17) such as PKCi, CHAMP1, BCKDK, MYEF2, PRCKa and PLEC, among others (**Supplementary File S4**).

Functional phosphorylation events are targetable by FDA-approved drugs

Given that identified phosphorylations might be functionally redundant or non-functional (5, 18), we sought to unravel those most likely to contribute to tumor pathobiology. To this end, we compared our phosphopeptide data with the functionality analysis of Ochoa and colleagues (2020) (18), and determined that out of the 600 significantly regulated phosphopeptides 230 are most likely functional (score >0.5) (**Fig. S2D**). Next, we annotated the functional up-regulated phosphopeptides by their predicted kinases to find the most relevant kinases in renal cancer (**Fig. 4A**). This revealed that CDK1, PAK2, p38d (MAPK12), JNK1 and p38b (MAPK11) are the kinases responsible for most of the functional phosphorylations in ccRCC tumors (**Fig. 4A** and **Supplementary File S4**). Since kinases are the major targets for cancer drugs (6), we further annotated the predicted kinases by their inhibitory FDA-approved drugs. Indeed, approximately 77% of the activated kinases (41 out of 53) are druggable (**Fig. S2E**). A subnetwork for the three most relevant kinases with the indication of functional phosphorylations (black font) is shown in **Fig. S5A**. While PAK2 and CDK1 can be targeted by the tyrosine kinase inhibitor fostamatinib, JNK1 can be inhibited by tamoxifen and minocycline. Furthermore, cell viability assays showed for tamoxifen (**Fig. S5E**), which targets besides JNK1 several PKC kinases (**Supplementary File S4**) a significant toxic effect on CAKI-2 as well as A498 cells at low concentrations (p-value <0.05). Both kinase groups were previously reported to increase proliferation and invasiveness of ccRCC cells (30, 31). Tamoxifen is widely used for breast cancer treatment (32) and our results support the efficacy of this drug for ccRCC as a similar cell viability was determined between A498 cells and MCF7 cells (**Fig. S5E**). Moreover, 22 out of the 53 kinases in **Fig. 4A** have a prognostic value for ccRCC tumors based on TCGA-KIRC follow-up data (n=530 patients) including several CDKs such as CDK1,

Journal Pre-proof

CDK2, CDK3, CDK4 and CDK5, as well as several MAPKs such as MAPK11, MAPK13, MAPK7 and MAP2K2 (**Fig. S3**), which stresses the importance to investigate cell proliferation related pathways. Furthermore, CPTAC follow-up data showed for PAK2, CDK4, PKCa and CLK4 significantly worse survival outcome (log-rank test, *p*-value <0.05) for the global proteome (**Fig. S4A**) and phosphoproteome data (**Fig. S4B**) of ccRCC patients, respectively, due to high expression of these kinases in the tumor tissues compared to NATs.

A summary of the most elevated signaling pathways orchestrated by phosphorylation in ccRCC tumors and relevant kinase inhibitors is illustrated in **Fig. 4B**.

Discussion

In this study, we identified 16,253 phosphopeptides on 3,486 proteins by quantitative phosphoproteomics analysis of ccRCC tissues and NATs (**Fig. 1C**). Comparison with other high-throughput approaches to characterize the ccRCC phosphoproteome revealed a high level of concordance between our study and the CPTAC phosphoproteome (**Fig. S5B and S5C**). Approximately 66% of the identified phosphosites of this study are shared with the CPTAC dataset. In total, 6,775 quantified common phosphosites displayed a significant positive correlation (0.54, *p*-value <0.05, **Fig. S5C**) between both datasets. More than 3,700 phosphosites are unique to our study suggesting previously undescribed observations of phospho signal transduction in ccRCC such as ion homeostasis, microtubule polymerization/depolymerization, protein localization, wound healing and cell-cell junction assembly (**Supplementary File S2**). These phosphosites might have been caught due to the different phosphopeptide enrichment method, as we applied TiO_2-MOAC based enrichment, while the CPTAC group used Fe^{3+}-IMAC.

Our in-depth proteomics analysis predicted all 6 members of p21-activated kinases (PAKs) to be highly activated in the ccRCC tumors (**Fig. 3C**). PAKs are known to be switched on by the small GTPases Rac1 and Cdc42, and to be crucial for cytoskeletal dynamics, invasion,

Journal Pre-proof

metastasis, cell death and proliferation (33). Previous phosphoproteomics studies have not yet described PAKs as relevant kinases in ccRCC tumorigenesis (8-10), however, our data strongly indicates that especially PAK2 is highly functional in the tumors as it is predicted to phosphorylate 13 functional peptides across 7 different substrates (Tier II, **Fig. S5A**). In addition, PAK2 is one of the few kinases that has also been experimentally detected by our proteomics approach (**Supplementary Files S2 and S3**), supporting its predicted elevated activity. While especially the role of PAK1 is largely understood in different cancers, the function and targets of PAK2 remain to be elucidated (33, 34). Furthermore, PAK2 has previously been noted to bind to CDK12 and thereby to activate the MAPK pathway (34). Our study shows for CDK1 and CDK5 high activity (**Fig. 3A**), which warrants further investigation to shed light into the synergistic functionality of PAKs and CDKs regarding cell cycle regulation in RCC. Moreover, both PAKs and CDKs have been linked to hypoxia, which is one of the main characteristics of ccRCC tumors (11, 35). More specifically, increased levels of PAKs are caused by hypoxia-induced activation of the mediators Rac1 and Cdc42 through phosphatidylinositol 3 kinase (PI3K) and protein tyrosine kinase (PTK) (**Fig. 4B** and (36)). In contrast, CDKs are indirect downstream effectors of hypoxia as they are interactors of the hypoxia-induced cell cycle proteins Cyclin D1, Cyclin A and Cyclin E, respectively (37). Furthermore, we determined for PAK5, PAK6, CDK1, CDK2, CDK3, CDK4 and CDK5 worse survival outcome at high expression levels based on TCGA-KIRC mRNA data (**Fig. S3**). Additionally, survival analysis based on both CPTAC proteome as well as phosphoproteome data revealed that PAK2 has a prognostic value for ccRCC patients (**Fig. S4**). Moreover, our analysis suggests that all PAKs can be inhibited by the tyrosine kinase inhibitor fostamatinib (**Fig. 4B**). It is worthwhile to examine the efficacy of fostamatinib in ccRCC treatment along with inhibitors for other signaling components such as CDKs and MAPKs as combinatorial anti-cancer strategy.

Another highly up-regulated phosphoprotein in the tumor tissues is the receptor tyrosine kinase EGFR. We have already described the potential involvement of the oncogenic EGFR-MAPK

Journal Pre-proof

and EGFR-AKT1-mTOR axes, which are known to drive proliferation, inflammation, survival and metastasis, in our global proteome analysis of the same tissue samples (8, 11). EGFR has been reported to be overexpressed in RCC tumors, however, no clinically approved drug against EGFR is currently in use for RCC treatment (8, 10). Our data suggests that EGFR is a substrate of different predicted kinases such as PDK1, MAPK1, MAPK3, GRK2, CaMK2a and CaMK2g (Tier II, **Fig. S5D**). We identified 2 significantly up-regulated phosphosites for EGFR, namely T693 and S1166, which are predicted to be functional modifications. EGFR is particularly known to be activated by tyrosine phosphorylations in its tyrosine kinase domain (713-965 aa) (**Fig. S5D**) (4), however, we could not detect sites in this domain probably due to the intrinsic nature of our enrichment method to primarily catch serine and threonine residues. Based on our findings, we propose that both the experimentally derived EGFR-mediated pathways, as well as the predicted VEGFR-mediated signaling cascades are likely to synergistically govern malignant phospho signaling in ccRCC tumors (**Fig. 4B**).

As indicated by our data, the hyperphosphorylation of intermediate filaments such as vimentin or keratins is a major event in ccRCC tumors (**Fig. 3C, Supplementary File S2**), which further supports the suggested migratory behavior of renal cancers (27, 38). It has been previously described that the levels of vimentin are four times higher in ccRCC, while the epithelial marker E-cadherin is expressed at half or only one third of the level compared to 5 other cancer types (7). This may provide a possible explanation for the fact that around one third of ccRCC patients already display distant metastasis at diagnosis (7). As with other epithelial carcinomas, keratins are also used as biomarkers for the accurate classification of renal cell carcinomas (39). ccRCC tumors mainly express KRT7, KRT8, KRT18 and KRT19 (39). Our analysis identified multiple up-regulated keratin phosphorylation sites, including KRT8 and KRT19, in ccRCC tumors (Tier II). These phosphorylated proteoforms of keratins may serve as valuable biomarkers in immunohistochemistry for sub-classification of renal cancers.

Overall, our comprehensive phosphoproteomics profiling of ccRCC tissues shed new light on the signaling cascades driving renal tumorigenesis. Current approved treatment regimes for

advanced tumors use the tyrosine kinase inhibitors (TKIs) sunitinib, pazopanib, cabozantinib, axitinib and sorafenib against VEGFR in the first-line setting (40). Furthermore, recent trials combining TKIs with immunotherapeutics such as axitinib with pembrolizumab or with avelumab showed better toleration and median survival outcome than monotherapies (40). However, many trials have failed to effectively target other important mediators of RCC tumorigenesis such as EGFR (8, 10), which is also supported by our data to be a central player alongside VEGFR. Hence, future directions warrant the investigation of new targeted therapies against EGFR and its downstream effectors PAK and CDK kinases with the suggested agents fostamatinib and minocycline, also as combinatorial treatments with approved EGFR agents such as dacomitinib, cetuximab and erlotinib.

Data Availability

This article contains supplemental data. The mass spectrometry proteomics data have been deposited to the ProteomeXchange Consortium via the PRIDE (41) partner repository with the dataset identifier PXD028428.

Acknowledgements

We gratefully acknowledge the KUPAM and KUTTAM OMICS facilities of Koc University, especially Busra Akarlar and Nazli Ezgi Ozkan Kucuk for their technical support. We thank Ozgur Kurt from Koc University School of Medicine for his essential help in pathological assessment of tissue samples, and Isin Kilicaslan and Yasemin Ozluk from Istanbul University Istanbul Faculty of Medicine for their supervisory contribution during pathological assessment of tissue samples. The results shown here are in whole or part based upon data generated by the TCGA Research Network: https://www.cancer.gov/tcga. Data used in this publication were generated by the Clinical Proteomic Tumor Analysis Consortium (NCI/NIH).

Author Contributions

A.S. and N.O. designed the research plan. A.S. performed proteomics experiments, statistical analysis, data analysis and data visualization. A.T.S. performed cell viability assay and related data visualization. A.A. performed H&E staining of tissue samples. S.B. performed pathological assessment of tissues. O.A., M.C.K., S.E., A.A. and T.E. consulted on clinical questions. N.O. conceived and supervised the study. A.S. wrote the manuscript with inputs from N.O. and A.T.S. All authors discussed the results and commented on the manuscript.

References

1. Craven RA, Vasudev NS, Banks RE. Proteomics and the search for biomarkers for renal cancer. Clin Biochem. 2013;46(6):456-65.
2. Capitanio U, Montorsi F. Renal cancer. The Lancet. 2016;387(10021):894-906.
3. J. Cooper S, W. Tun H, M. Roper S, Kim Y. Current Status of Biomarker Discovery in Human clear Cell Renal Cell Carcinoma. Journal of Molecular Biomarkers & Diagnosis. 2012;01(S2).
4. Ardito F, Giuliani M, Perrone D, Troiano G, Lo Muzio L. The crucial role of protein phosphorylation in cell signaling and its use as targeted therapy (Review). Int J Mol Med. 2017;40(2):271-80.
5. Humphrey SJ, James DE, Mann M. Protein Phosphorylation: A Major Switch Mechanism for Metabolic Regulation. Trends Endocrinol Metab. 2015;26(12):676-87.
6. Harsha HC, Pandey A. Phosphoproteomics in cancer. Mol Oncol. 2010;4(6):482-95.
7. Deb B, Sengupta P, Sambath J, Kumar P. Bioinformatics Analysis of Global Proteomic and Phosphoproteomic Data Sets Revealed Activation of NEK2 and AURKA in Cancers. Biomolecules. 2020;10(2).
8. Clark DJ, Dhanasekaran SM, Petralia F, Pan J, Song X, Hu Y, et al. Integrated Proteogenomic Characterization of Clear Cell Renal Cell Carcinoma. Cell. 2019;179(4):964-83 e31.
9. Peng X, Xu F, Liu S, Li S, Huang Q, Chang L, et al. Identification of Missing Proteins in the Phosphoproteome of Kidney Cancer. J Proteome Res. 2017;16(12):4364-73.
10. Haake SM, Li J, Bai Y, Kinose F, Fang B, Welsh EA, et al. Tyrosine Kinase Signaling in Clear Cell and Papillary Renal Cell Carcinoma Revealed by Mass Spectrometry-Based Phosphotyrosine Proteomics. Clin Cancer Res. 2016;22(22):5605-16.
11. Senturk A, Sahin AT, Armutlu A, Kiremit MC, Acar O, Erdem S, et al. Quantitative Proteomics Identifies Secreted Diagnostic Biomarkers as well as Tumor-Dependent Prognostic Targets for Clear Cell Renal Cell Carcinoma. Mol Cancer Res. 2021;19(8):1322-37.

12. Zhou H, Ye M, Dong J, Corradini E, Cristobal A, Heck AJ, et al. Robust phosphoproteome enrichment using monodisperse microsphere-based immobilized titanium (IV) ion affinity chromatography. Nat Protoc. 2013;8(3):461-80.
13. Kall L, Canterbury JD, Weston J, Noble WS, MacCoss MJ. Semi-supervised learning for peptide identification from shotgun proteomics datasets. Nat Methods. 2007;4(11):923-5.
14. Mi H, Muruganujan A, Ebert D, Huang X, Thomas PD. PANTHER version 14: more genomes, a new PANTHER GO-slim and improvements in enrichment analysis tools. Nucleic Acids Res. 2019;47(D1):D419-D26.
15. Sondka Z, Bamford S, Cole CG, Ward SA, Dunham I, Forbes SA. The COSMIC Cancer Gene Census: describing genetic dysfunction across all human cancers. Nat Rev Cancer. 2018;18(11):696-705.
16. Wishart DS, Feunang YD, Guo AC, Lo EJ, Marcu A, Grant JR, et al. DrugBank 5.0: a major update to the DrugBank database for 2018. Nucleic Acids Res. 2018;46(D1):D1074-D82.
17. Uretmen Kagiali ZC, Sanal E, Karayel O, Polat AN, Saatci O, Ersan PG, et al. Systems-level Analysis Reveals Multiple Modulators of Epithelial-mesenchymal Transition and Identifies DNAJB4 and CD81 as Novel Metastasis Inducers in Breast Cancer. Mol Cell Proteomics. 2019;18(9):1756-71.
18. Ochoa D, Jarnuczak AF, Vieitez C, Gehre M, Soucheray M, Mateus A, et al. The functional landscape of the human phosphoproteome. Nat Biotechnol. 2020;38(3):365-73.
19. Horn H, Schoof EM, Kim J, Robin X, Miller ML, Diella F, et al. KinomeXplorer: an integrated platform for kinome biology studies. Nat Methods. 2014;11(6):603-4.
20. Binns D, Dimmer E, Huntley R, Barrell D, O'Donovan C, Apweiler R. QuickGO: a web-based tool for Gene Ontology searching. Bioinformatics. 2009;25(22):3045-6.
21. Liao Y, Wang J, Jaehnig EJ, Shi Z, Zhang B. WebGestalt 2019: gene set analysis toolkit with revamped UIs and APIs. Nucleic Acids Res. 2019;47(W1):W199-W205.
22. Eid S, Turk S, Volkamer A, Rippmann F, Fulle S. KinMap: a web-based tool for interactive navigation through human kinome data. BMC Bioinformatics. 2017;18(1).
23. Cheng A, Grant CE, Noble WS, Bailey TL. MoMo: discovery of statistically significant post-translational modification motifs. Bioinformatics. 2019;35(16):2774-82.
24. Gyorffy B, Lanczky A, Eklund AC, Denkert C, Budczies J, Li Q, et al. An online survival analysis tool to rapidly assess the effect of 22,277 genes on breast cancer prognosis using microarray data of 1,809 patients. Breast Cancer Res Treat. 2010;123(3):725-31.
25. Cancer Genome Atlas Research N. Comprehensive molecular characterization of clear cell renal cell carcinoma. Nature. 2013;499(7456):43-9.
26. Hornbeck PV, Zhang B, Murray B, Kornhauser JM, Latham V, Skrzypek E. PhosphoSitePlus, 2014: mutations, PTMs and recalibrations. Nucleic Acids Res. 2015;43(Database issue):D512-20.
27. Sharma P, Alsharif S, Fallatah A, Chung BM. Intermediate Filaments as Effectors of Cancer Development and Metastasis: A Focus on Keratins, Vimentin, and Nestin. Cells. 2019;8(5).
28. Kamacioglu A, Tuncbag N, Ozlu N. Structural analysis of mammalian protein phosphorylation at a proteome level. Structure. 2021.
29. Rust HL, Thompson PR. Kinase consensus sequences: a breeding ground for crosstalk. ACS Chem Biol. 2011;6(9):881-92.
30. Brenner W, Färber G, Herget T, Wiesner C, Hengstler JG, Thüroff JW. Protein kinase C eta is associated with progression of renal cell carcinoma (RCC). Anticancer Res. 2003;23(5A):4001-6.
31. An J, Liu H Fau - Magyar CE, Magyar Ce Fau - Guo Y, Guo Y Fau - Veena MS, Veena Ms Fau - Srivatsan ES, Srivatsan Es Fau - Huang J, et al. Hyperactivated JNK is a therapeutic target in pVHL-deficient renal cell carcinoma. (1538-7445 (Electronic)).
32. Osborne CK. Tamoxifen in the Treatment of Breast Cancer. New England Journal of Medicine. 1998;339(22):1609-18.
33. Ye DZ, Field J. PAK signaling in cancer. Cell Logist. 2012;2(2):105-16.
34. Liu H, Liu K, Dong Z. The Role of p21-Activated Kinases in Cancer and Beyond: Where Are We Heading? Front Cell Dev Biol. 2021;9:641381.
35. Rini BI, Campbell SC, Escudier B. Renal cell carcinoma. The Lancet. 2009;373(9669):1119-32.

36. Xue Y, Bi F, Zhang X, Zhang S, Pan Y, Liu N, et al. Role of Rac1 and Cdc42 in hypoxia induced p53 and von Hippel-Lindau suppression and HIF1alpha activation. Int J Cancer. 2006;118(12):2965-72.
37. Druker J, Wilson JW, Child F, Shakir D, Fasanya T, Rocha S. Role of Hypoxia in the Control of the Cell Cycle. Int J Mol Sci. 2021;22(9).
38. Sawant MS, Leube RE. Consequences of Keratin Phosphorylation for Cytoskeletal Organization and Epithelial Functions. Int Rev Cell Mol Biol. 2017;330:171-225.
39. Karantza V. Keratins in health and cancer: more than mere epithelial cell markers. Oncogene. 2011;30(2):127-38.
40. Chowdhury N, Drake CG. Kidney Cancer: An Overview of Current Therapeutic Approaches. Urol Clin North Am. 2020;47(4):419-31.
41. Perez-Riverol Y, Csordas A, Bai J, Bernal-Llinares M, Hewapathirana S, Kundu DJ, et al. The PRIDE database and related tools and resources in 2019: improving support for quantification data. Nucleic Acids Res. 2019;47(D1):D442-D50.
42. Brannon AR, Reddy A, Seiler M, Arreola A, Moore DT, Pruthi RS, et al. Molecular Stratification of Clear Cell Renal Cell Carcinoma by Consensus Clustering Reveals Distinct Subtypes and Survival Patterns. Genes Cancer. 2010;1(2):152-63.

Figure legends

Figure 1. Phosphoproteome analysis of clear cell Renal Cell Carcinoma. (A) Experimental outline of dimethylation-based quantitative phosphoproteomics approach. **(B)** Distribution of quantified phospho- and non-phosphopeptides across all patients. **(C)** Number of identified and quantified phosphopeptides and phosphoproteins. “Quantified” refers to quantifications in at least 2 out of 3 technical replicates. **(D)** MA plot depicting intensity distribution of quantified phospho- and non-phosphopeptides. Top and right histograms show distribution of fold change values and intensities of non-phosphopeptides, respectively, with density lines representing theoretical normal distribution. **(E)** Histogram showing general distribution of median tumor/normal ratios of quantified phospho- and non-phosphopeptides. Student’s *t*-test was applied for statistical determination of skewness between distributions, p-value <0.05. **(F)** Frequency distribution of identified serine (pSer), threonine (pThr) and tyrosine (pTyr) phosphosites with ≥50% localization probability. **(G)** Frequency distribution of identified singly (1P site) and multiply (≥ 2P sites) phosphorylated peptides with ≥50% site probability. **(H)**

Comparison of identified phosphosites with ≥50% localization probability with PhosphoSitePlus database.

Figure 2. Significantly regulated phosphorylations in ccRCC. (A) Overview of the number of quantified phosphopeptides. Inner pie chart represents number of significantly regulated phosphopeptides with the majority being up-regulated in the tumor tissues. **(B)** Volcano plot depicting significantly regulated phosphopeptides. **(C)** Enriched biological processes in ccRCC tumors compared to adjacent normal tissues. Top 10 PANTHER GO-Slim biological process annotations of significantly up-regulated (pink) and down-regulated (blue) phosphoproteins, respectively. **(D)** Corresponding regulation of significantly regulated phosphoproteins in global proteome of same ccRCC tissues as described in (11). **(E)** Scatter plot depicting distribution of matching phosphopeptides with non-phosphorylated counterpart of global proteome. Indication of matches associated with significant protein abundance changes in global proteome in light green. **(F)** Tumor/normal fold change distributions of significantly regulated phosphopeptides with respective non-phosphorylated counterpart. For statistical evaluation of distribution, BH-adjusted *p*-value correction was applied after one-sample Wilcoxon signed-rank test. **(G-H)** Enriched consensus motifs of significantly regulated serine and threonine phosphopeptides sorted by their ascending *p*-value (gradient coloring). Phosphosites with ≥50% probability (centered to the phospho residue and enlarged by the ±7 aa sequence window) were used for the analysis with the motif-x algorithm.

Figure 3. Altered kinase activities in ccRCC tumors. (A) Predicted activated and reduced kinases in the tumor tissues compared to NATs according to the NetworKIN3.0 tool. Top 10 kinases with highest number of predictions are shown (with gradient coloring representing ranking). Average NetworKIN scores of predictions are shown as bar labels. **(B)** Human kinome tree of activated and reduced kinases in ccRCC tumors. The web tool KinHub was used with indications of predicted kinases associated with significantly up-regulated (42), up- and down-regulated (yellow), and down-regulated (blue) phosphopeptides, respectively. **(C)** Kinase-substrate network depicting the most enriched Reactome pathways (Tier II data). Nodes are organized by their cellular compartment retrieved using the QuickGO web tool. Enrichment level of pathways decreases from left to right. Mesenchymal phosphorylations (orange border) as well as the role of substrates in cancer (node font color) are also indicated. Incomplete node border indicates Tier II (quantified in ≥50% of cohort), while complete border refers to Tier I (quantified in ≥75% of cohort).

Journal Pre-proof

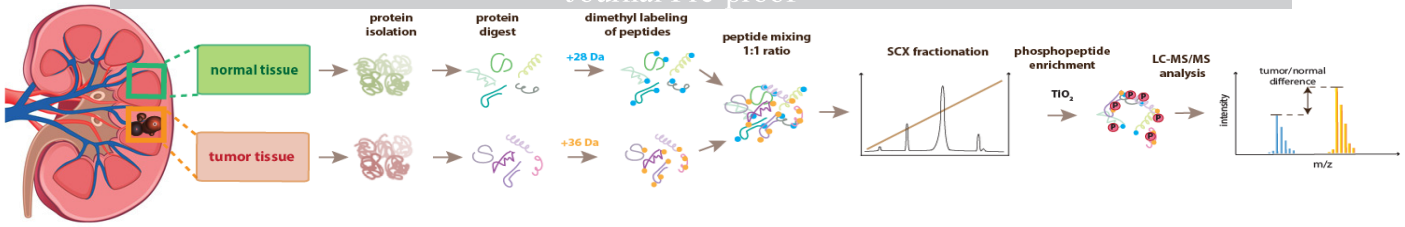
652 **Figure 4. Altered kinase activities in ccRCC tumors. (A)** Predicted activated kinases
653 associated with significantly up-regulated phosphopeptides with a functional score >0.5
654 according to Ochoa *et al.* (2020). Indicated drugs are associated FDA-approved therapeutics
655 with inhibitor function (for full drug list see Supplementary File S4). The prognostic feature of
656 the kinases refers to Fig. S3. **(B)** Summarized significantly enriched phosphorylated pathways
657 in ccRCC tumor tissues targetable with FDA-approved drugs (Tier II data). Enrichment level of
658 pathways decreases from left to right. Signaling events that are predicted according to
659 literature are shown in grey. Tier II nodes (quantified in ≥50% of cohort) are indicated with
660 brighter colours.

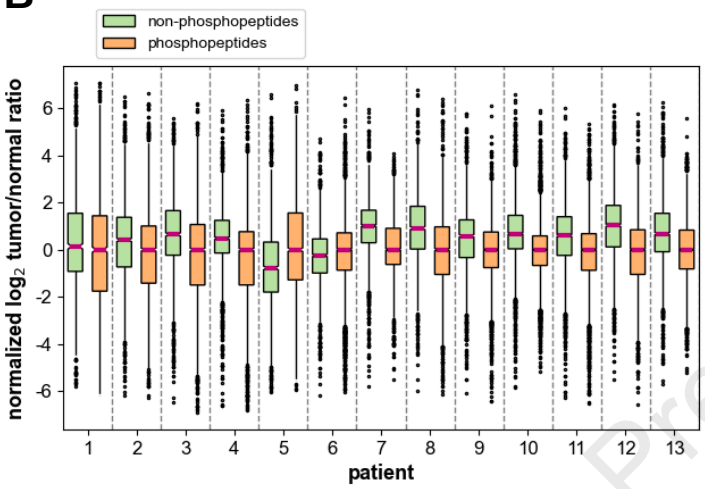
661

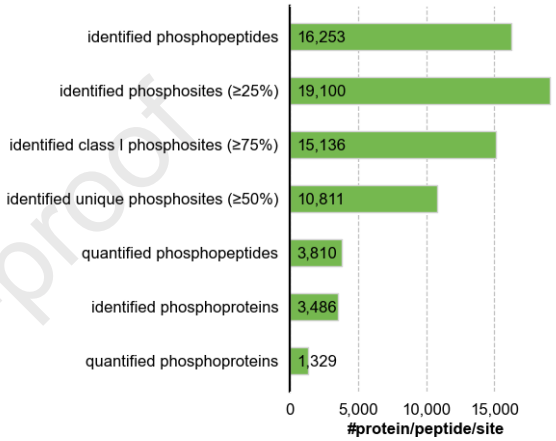
Journal Pre-proof

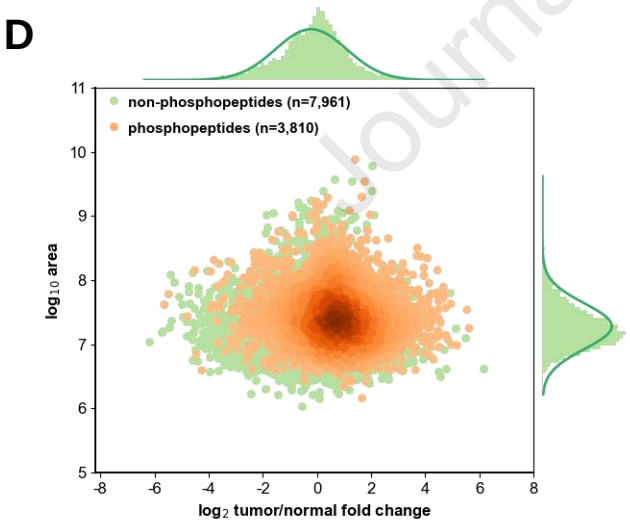
Figure 1

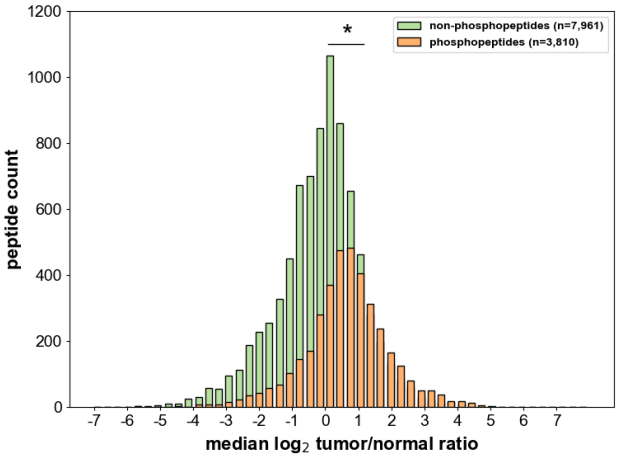
Journal Pre-proof

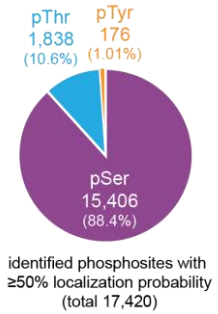


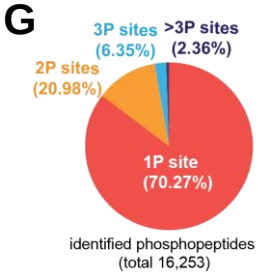












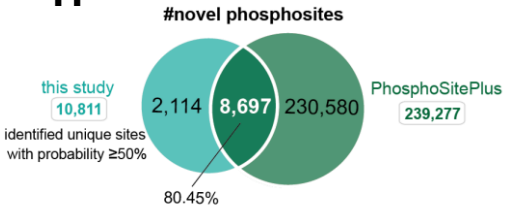


Figure 2

Journal Pre-proof

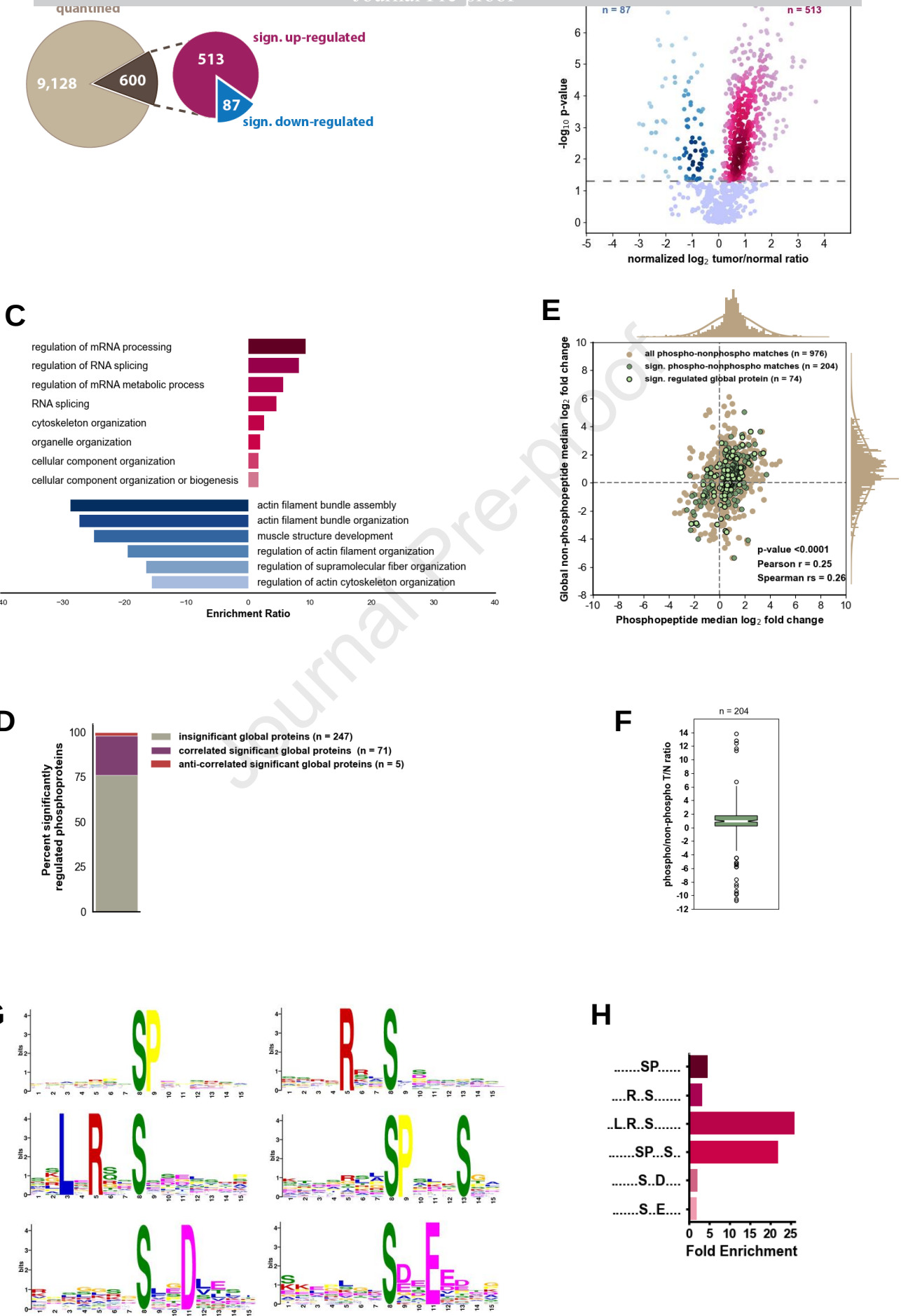
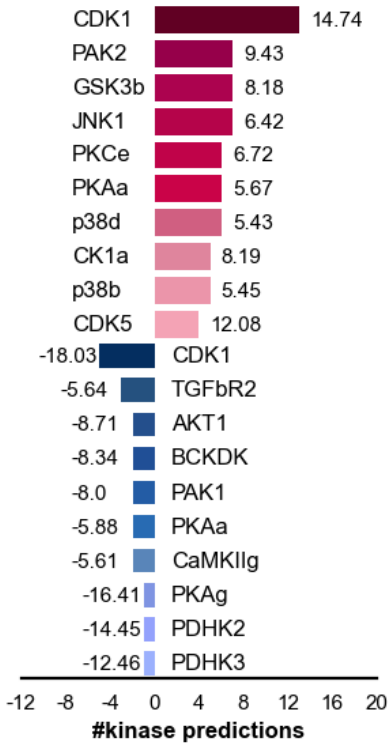
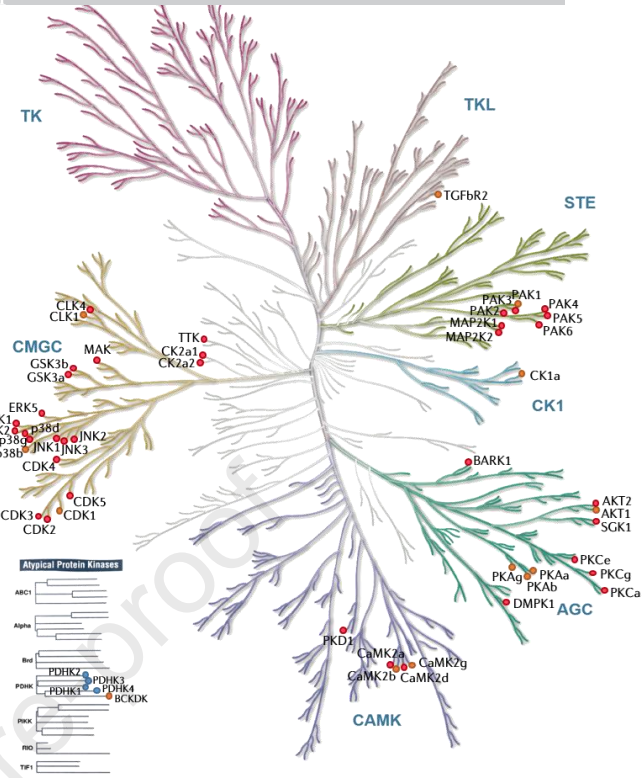


Figure 3

Journal Pre-proof

A





Journal Pre-proof

C

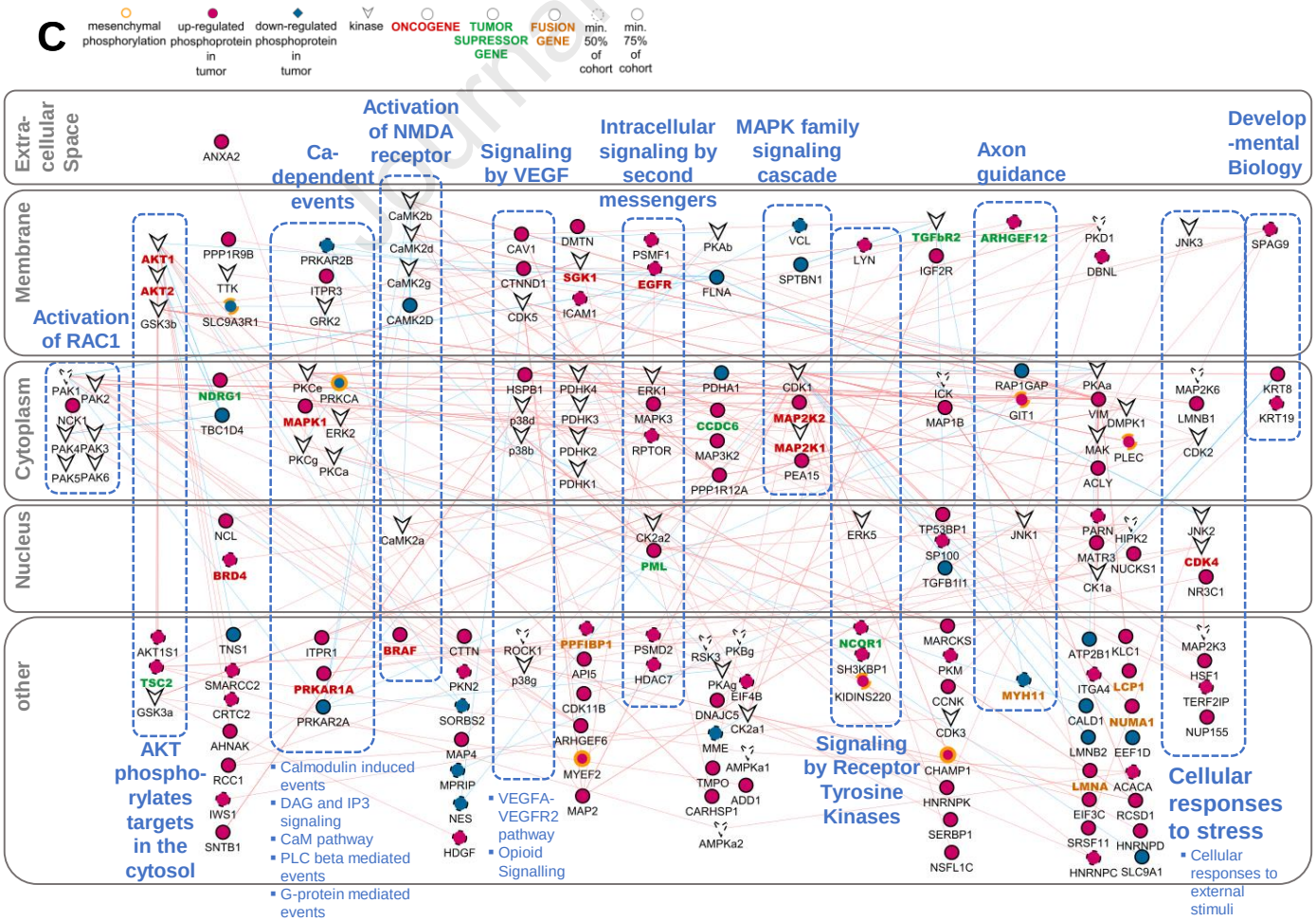
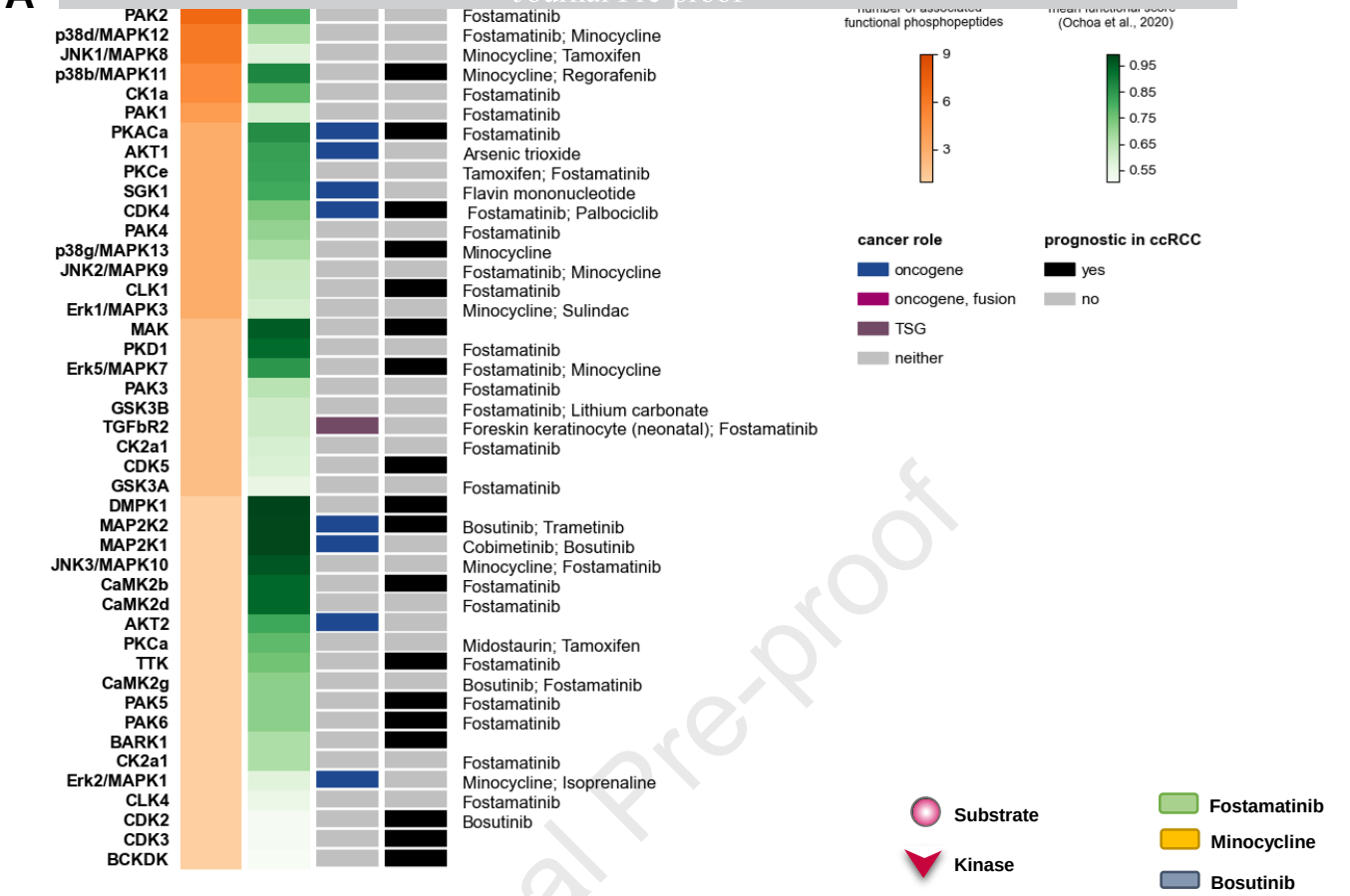
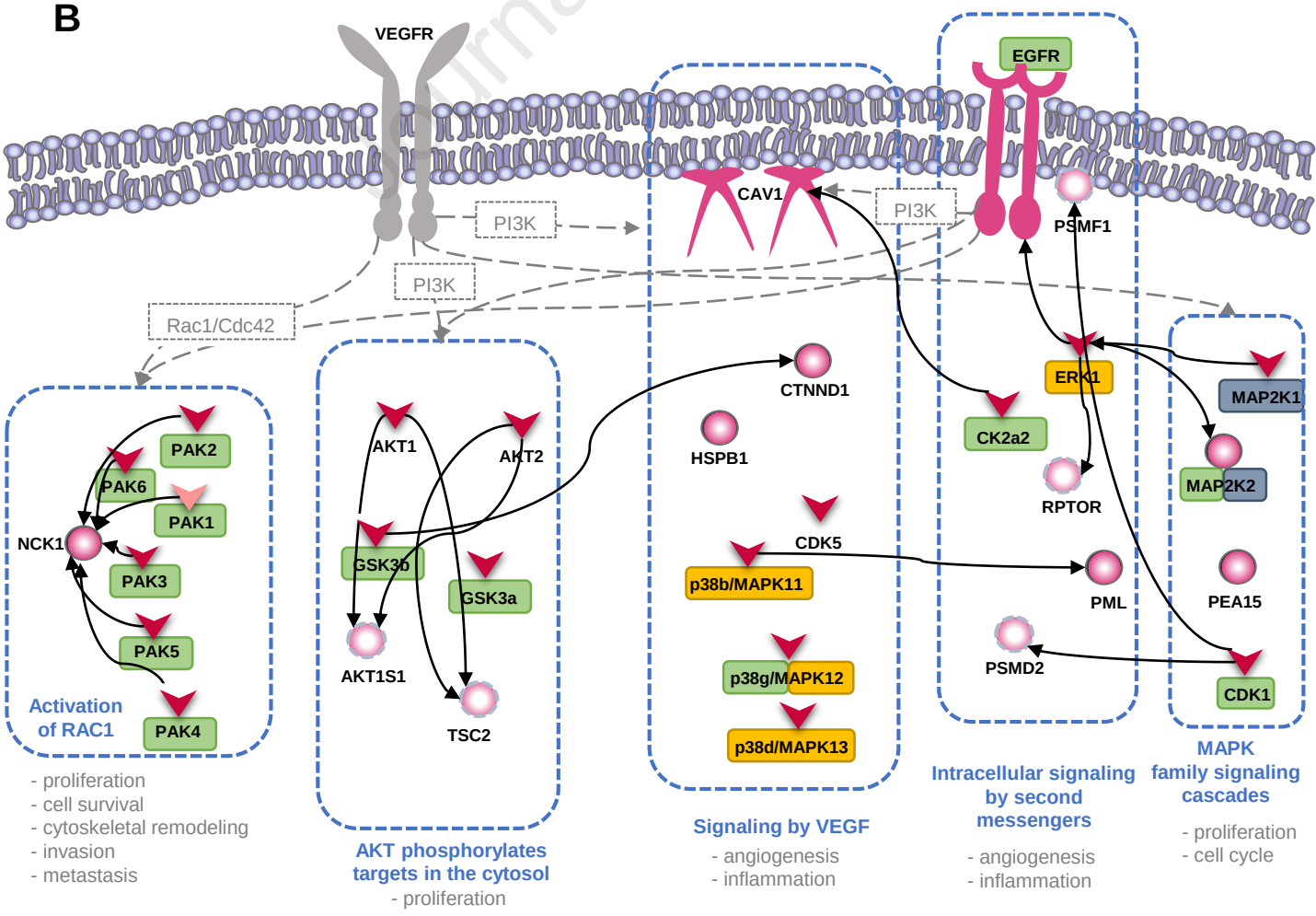


Figure 4

Journal Pre-proof





Journal Pre-proof

Highlights

- Quantitative phosphoproteomics approach using TiO_2-MOAC identified more than 16,000 phosphopeptides from ccRCC tumor and NAT samples
- Mesenchymal profile of detected phosphoproteins and enrichment of cytoskeletal elements imply increased migratory and invasive behavior of ccRCC tumors
- PAK2 and CDK1 are undescribed key kinases in ccRCC tumorigenesis and are targets of the FDA-approved inhibitory drugs fostamatinib, minocycline, tamoxifen and pseudoephedrine which are currently not used in RCC treatment
- High expression of PAK2 leads to significantly worse survival of ccRCC patients

Journal Pre-proof

Journal Pre-proof

Brief

Senturk *et al.* (2022) applied quantitative dimethyl-based phosphoproteomics analysis on ccRCC tumor and normal adjacent tissue (NAT) samples. The in-depth analysis led to the identification of more than 16,000 phosphopeptides of which 1,336 were determined as significantly regulated between tumors and NATs. Kinase-substrate network analysis revealed that several oncogenic pathways are enriched in the tumors such as Rac1 activation, MAPK and VEGF signaling, EGFR signaling and cytokine signaling. The previously for ccRCC undescribed group of PAK kinases has been identified as the most up-regulated kinases associated with functional phosphorylations in the tumors. Among these kinases, PAK2 displayed prognostic value for ccRCC patients and is one the key kinases in ccRCC pathogenesis driving tumor migration and invasion.

Journal Pre-proof

Journal Pre-proof

Declaration of interests

☒ The authors declare that they have no known competing financial interests or personal relationships that could have appeared to influence the work reported in this paper.

☐The authors declare the following financial interests/personal relationships which may be considered as potential competing interests:

Journal Pre-proof

Author Contributions

A.S. and N.O. designed the research plan. A.S. performed proteomics experiments, statistical analysis, data analysis and data visualization. A.T.S. performed cell viability assay and related data visualization. A.A. performed H&E staining of tissue samples. S.B. performed pathological assessment of tissues. O.A., M.C.K., S.E., A.A. and T.E. consulted on clinical questions. N.O. conceived and supervised the study. A.S. wrote the manuscript with inputs from N.O. and A.T.S. All authors discussed the results and commented on the manuscript.

Journal Pre-proof